Multimodal output mapping of human central motor representation on different spatial scales

Joseph Classen *, Uwe Knorr †, Konrad J. Werhahn ‡, Gottfried Schlaug §, Erwin Kunesch *, Leonardo G. Cohen ‖, Rüdiger J. Seitz † and Reiner Benecke *

*Zentrum für Nervenheilkunde, Neurologische Klinik, Universität Rostock, †Neurologische Klinik, Heinrich-Heine-Universität, Düsseldorf, ‡Neurologische Klinik, Klinikum Großhadern, Ludwig-Maximilians-Universität München, Germany, §Beth Israel Deaconess Medical Center, Harvard Medical School, Boston, MA and ‖Human Cortical Physiology Unit, Medical Neurology Branch, NINDS, Bethesda, MD, USA

(Received 11 December 1997; accepted after revision 22 June 1998)

1. Non-invasive mapping by focal transcranial magnetic stimulation (TMS) is frequently used to investigate cortical motor function in the intact and injured human brain. We examined how TMS-derived maps relate to the underlying cortical anatomy and to cortical maps generated by functional imaging studies.

2. The centres of gravity (COGs) of TMS maps of the first dorsal intersosseus muscle (FDI) were integrated into 3-D magnetic resonance imaging (MRI) data sets in eleven subjects. In seven of these subjects the TMS-derived COGs were compared with the COG of regional cerebral blood flow increases using positron emission tomography (PET) in an index finger flexion protocol.

3. Mean TMS-derived COG projections were located on the posterior lip of the precentral gyrus and TMS-derived COG projections were in close proximity to the mean PET-derived COG, suggesting that the two methods reflect activity of similar cortical elements.

4. Criteria for a reliable assessment of the COG and the number of positions with a minimum amplitude of two-thirds of the maximum motor-evoked potential (T3Ps) were determined as a function of the number of stimuli and extension of the stimulation field. COGs and T3Ps were compared with an estimate of the size of the human motor cortex targeting α-motoneurons of forearm muscles. This comparison suggests that TMS can retrieve spatial information on cortical organization below the macroanatomic scale of cortical regions.

5. Finally, we studied the cortical representation of hand muscles in relation to facial and foot muscle representations and investigated hemispherical asymmetries. We did not find any evidence for a different ipsi- or contralateral representation of the mentalis muscle. Also, no difference was found between FDI representations on the dominant *versus* the non-dominant hemisphere.

A variety of mapping techniques have been successfully applied to investigate the plasticity of the human motor system associated with lesions of the nervous system (Ojemann & Silbergeld, 1995; Seitz *et al.* 1995; Rijntjes *et al.* 1997) or motor learning in healthy subjects (Schlaug *et al.* 1994; Karni *et al.* 1995; Pascual-Leone *et al.* 1995; Cohen *et al.* 1996). Furthermore, mapping is used to determine the site of the primary motor cortex in surgical patients (Yousry *et al.* 1995). While the most direct information is provided by intraoperative brain stimulation, it is apparent that such invasive methods can only be used during open brain surgery. Of the various non-invasive and safe techniques, each one is sensitive to different and specific aspects of the physiology of the motor system, but transcranial magnetic stimulation (TMS) mapping is unique in quickly providing direct information on the neuronal circuitry relating to motor output. Several studies have attempted to enhance and complement information derived from a single mapping technique by integrating multiple methods describing functional as well as structural aspects of the motor system. Such multimodal integration is inherent in functional magnetic resonance imaging (fMRI) studies (Rao *et al.* 1995), and has also been attempted using electroencephalography (EEG) or magnetoencephalography (MEG) (Walter *et al.*

1992) and positron emission tomography (PET) imaging (Steinmetz *et al.* 1992). Only a few studies exist which relate TMS mapping results to the underlying anatomy (Levy *et al.* 1991; Wang *et al.* 1994; Wassermann *et al.* 1996; Krings *et al.* 1997) and only recently have TMS mapping results been compared with functional activation studies (Wassermann *et al.* 1996; Krings *et al.* 1997). In general, these studies have shown that motor representations are similar with different techniques. However, it remains unclear to what degree non-invasive human motor cortical output mapping using TMS and studies of cerebral blood flow activation (PET) co-validate each other.

This question was addressed in the present study. In addition, we examined whether TMS mapping can resolve spatial details of the distribution of excitability within the cortex below the macroanatomical scale of cortical regions. Furthermore, mapping of muscles of the face, hand and foot on both hemispheres allowed us to address bilaterality of facial muscle representation and representations of dominant *versus* non-dominant hand muscles.

Some of the results have been published previously in abstract form (Classen *et al.* 1995).

METHODS

Experiments were approved by the Ethics Committee of the University of Düsseldorf and complied with the Declaration of Helsinki. Informed written consent was obtained after the nature of the experimental procedures had been explained. Fourteen subjects (11 male, 3 female, mean age 28·8 ± 5·2 years) participated in the study. All subjects except one, who was left-handed, were right-handed as assessed by the Edinburgh inventory (Oldfield, 1971).

Transcranial magnetic stimulation

Stimulation

Stimulation was performed with a flat 'figure-of-eight' coil (outer diameter of 1 wing, 7 cm; The Magstim Company, Whitland, Carmarthenshire, UK) connected to a magnetic stimulator (Magstim Model 200). The coil was held tangentially to the skull with the handle pointing posteriorly parallel to the mid-line. In two pilot experiments performed on peripheral nerves, the virtual cathode was found on the mid-line, 1 mm away from the junction of the two wings in a direction away from the handle. Stimulation co-ordinates are given with reference to this point.

Recording

Surface EMG recordings were obtained from one of the target muscles (first dorsal interosseus (FDI), 14 subjects; m. abductor hallucis (AH), 4 subjects; m. mentalis (MENT), 4 subjects) at rest as defined by absence of visible or audible EMG activity. EMG signals were recorded by Dantec surface electrodes, amplified using a Toennies Myograph IIR (Freiburg, Germany) with bandpass filtering of 20–3000 Hz and recorded with a gain of 100–500 μV division^{-1}. Motor-evoked potentials (MEPs) were digitized at a frequency of 5 kHz using a CED 1401 interface (Cambridge Electronic Design, Cambridge, UK) with standard software. Data were stored on a changeable hard disk for later off-line analysis.

Mapping

Subjects were seated comfortably in an armchair. The head was covered with an elastic gauze by which the hair was held flat on the skull. Cz was located at the vertex using the international 10–20 system and a flexible thin plastic grid with co-ordinates marked 1 cm apart from each other was attached to the scalp.

A provisional point of optimal excitability (pPOE) was determined at suprathreshold intensity (approximately 60% of maximal stimulator output for FDI, 80% for MENT, 100% for AH) by averaging approximately three stimuli each at various stimulation points.

The threshold for eliciting a MEP of at least 50 μV in at least three of five consecutive trials was determined at the pPOE with an accuracy of 2% of the stimulator output at a gain of 50–100 μV division^{-1}. After establishing the threshold intensity, sites adjacent to this point were stimulated in order to exclude the possibility that any more consistent or larger responses could be obtained. If any larger responses occurred the threshold was again determined at that point and the procedure was repeated.

The stimulus intensity during the mapping was set at 1·2 times the motor threshold intensity as measured at the pPOE.

FDI. In eleven subjects, magnetic stimulation was performed pseudorandomly in an area centred by the pPOE covering 7 cm × 7 cm on both cerebral hemispheres. If necessary, the area was enlarged in such a way that from the outermost stimulation sites no responses were obtained. Twenty stimuli were delivered at each site at a frequency of about 0·3 Hz as limited by the recharging time of the magnetic stimulator. Both hemispheres were studied. In six of the individuals experiments were performed in one session lasting about 4 h and in the remaining five subjects two sessions, between 7 and 52 days apart, were used.

In three additional subjects each of the stimuli was delivered pseudorandomly to the left hemisphere within an area of 7 cm × 7 cm until twenty stimuli had been applied at each of the forty-nine sites. If necessary, the area was enlarged as described above and at those additional points all twenty stimuli were delivered one after the other. In these subjects, mapping of the FDI was also performed, delivering a total of ten stimuli at each position while the subjects contracted the target muscle isometrically at a level of about 15% of the maximal voluntary force. Force was recorded by a strain gauge and displayed on an oscilloscope screen on which the individual 15% target force level was marked for visual feedback.

MENT and AH. For MENT and AH, 10 stimuli were delivered at each site of stimulation. The stimulation procedure was slightly varied, in that starting from pPOE, sites surrounding pPOE were stimulated and the field of stimulation was extended until no responses could be evoked in the target muscle. This resulted in at least thirty-seven (MENT) or thirty (AH) positions stimulated.

MR imaging and PET imaging

In twelve of the subjects who underwent TMS mapping of FDI, magnetic resonance (MR) imaging was performed in separate sessions. In seven of those subjects PET was also performed.

MR imaging

High-resolution MR scans were obtained with a 1·5 T Magnetom (Siemens, Erlangen, Germany) using a high-resolution 3-D fast low angle shot (FLASH) sequence. This sequence provides 128 contiguous sagittal images of 1·17 mm thickness with a 256 pixel ×

256 pixel matrix (pixel size, 1 mm × 1 mm) providing a volumetric data set of the entire head.

PET imaging

PET scanning was performed using an intravenous bolus injection of 40 mCi [^{15}O]butanol and the eight-ring GE Scanditronix PC4096 plus PET camera as detailed elsewhere (Herzog *et al.* 1996). This PET camera has an optimal spatial resolution of 4·6 mm in plane, and a slice distance of 6·5 mm (Rota Kops *et al.* 1990). For attenuation correction, a transmission scan was obtained prior to the emission scan using a rotating ^{68}Ge pin source. The fifteen PET image slices were reconstructed with a Hanning filter to an effective image resolution (FWHM) of 9·0 mm. The reconstructed images had a matrix of 128 × 128 pixels, 2·0 mm × 2·0 mm each.

The subject's head was placed into an individually moulded head support, and fixed with a plaster ribbon to minimize head movements during and between the measurements. The eyes were covered with pads and noise in the scanner room was minimized. The subject's hand was in a supinated position supported from below. The subject was instructed to flex and extend the right-hand index finger at a comfortable speed while the thumb and the 3rd, 4th and 5th finger were kept in a relaxed position. The frequency of flexion–extension movements was 1·9 ± 0·9 Hz (mean ± S.D.). Index finger flexion had been shown to invariably activate the FDI muscle in preliminary experiments. The activation was started at the time of tracer injection and was sustained over 100 s. The control condition was rest. PET scanning started at the time of the intravenous injection of [^{15}O]butanol into the right brachial vein, immediately flushed with 10 ml saline. The local tissue concentration in the brain was sampled in list mode.

Analysis

TMS mapping

Mean amplitudes were calculated for each site of stimulation and normalized to the largest mean amplitude obtained within the stimulation area unless stated otherwise. Three variables (number of top-third positions, optimal position and centre of gravity) were used to characterize amplitude maps and are defined below.

(a) The number of top-third positions (T3Ps) were defined as the number of those positions in which amplitudes of at least two-thirds of the maximal mean MEP amplitudes were elicited.

(b) The point of optimal excitability (POE) was defined as the co-ordinates of the site which evoked the maximal mean amplitude.

(c) The centre of gravity (COG) was calculated as the lateral co-ordinate at each position multiplied by the sum of the normalized mean amplitudes of all sites in the stimulation area with the same lateral co-ordinate, and summed over all lateral positions. The lateral co-ordinate of the COG was then obtained by dividing this value by the sum of all mean amplitudes. For the anteroposterior co-ordinate an analogous procedure was used.

Transformation of 2-D TMS co-ordinates into 3-D skull co-ordinates

Two-dimensional map co-ordinates were transformed into the 3-D anatomical co-ordinates of the MR data set using a multi-step algorithm and custom-made software as described previously (Steinmetz *et al.* 1989).

Anatomical landmarks (left preauricular point (PPL), right preauricular point (PPR), nasion and inion) were marked on sagittal

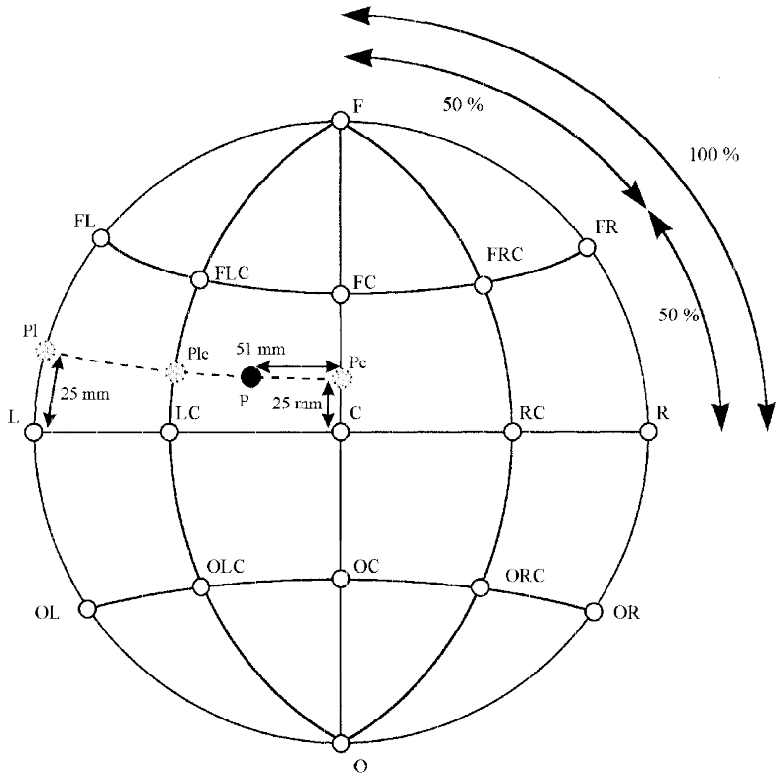

Figure 1. First step of the method of transformation of 2-D TMS co-ordinates into 3-D skull co-ordinates (schematic representation)

See Methods for an explanation of the lettering used.

slices using the volumetric MR data set (see above). Thereafter, on the sagittal slice containing the top-most point of the head, Cz* was marked. Cz was then calculated as the mid-point of the curve connecting inion and nasion through Cz*. In analogy to the 10–20 system, F, O and L, R were calculated as 40% of the distance starting from Cz along the nasion–Cz–inion line or along the PPL–Cz–PPR line, respectively. Several intermediate lines were made in order to minimize spatial errors when absolute distances were calculated on the skull surface in the MR data set (Fig. 1). The intermediate points FL, FC, FR, OL, OC and OR were defined at 50% of the distance along L–F, C–F, R–F, O–L, O–C and O–R, respectively. Similarly, FLC, FRC, OLC and ORC were found at 50% of the curved distance of LC–F, RC–F, O–LC and O–RC. To identify a point P corresponding to the 2-D COG co-ordinates of e.g. −51 mm lateral and 25 mm anterior on the MR skull surface, a curve with a constant distance of 25 mm parallel to the curve L–LC–C was constructed through the auxiliary points Pl, Plc and Pc (Fig. 1) in the modified co-ordinate system. On this curve, the point at the distance of 51 mm from the curve C–FC–F was calculated (Fig. 1).

Projection of COG into MR brain

At the skull site corresponding to the COG of the TMS amplitude map, a 3-D rod (diameter 3 pixels, or 3 mm) locally orthogonal to the surface of the skull was constructed and projected into the MR data set. To achieve local orthogonality the skull was spatially approximated by an ellipsoid constructed as follows: The intersection of the lines connecting F and O, and L and R (cf. Fig. 1) was defined as the centre of the ellipsoid. The orientation of the ellipsoid within the skull and its dimensions were determined by three half-diameters. The first half-diameter spanned from the centre of the ellipsoid to Cz, the second (orthogonal to the first) connected the centre of the ellipsoid with a point on the mid-sagittal plane through the nasion, and the third half-diameter was orthogonal to the first two and connected the centre of the ellipsoid with a point on the horizontal plane near L or R. The orthogonal COG projection was then constructed algebraically on the surface of the ellipsoid.

Using the Analyze image processing program (CNS Ltd, Southwater, UK) on three orthogonal projections, the sagittal, axial and coronal planes were identified where the rod representing the projection of the COG entered the brain. Using these three planes, the point where the COG projection entered the brain was identified and described in the stereotactic co-ordinates of Talairach & Tournoux (1988).

PET mapping

Analysis of PET images was performed using a multi-step algorithm described previously (Wunderlich *et al.* 1998). First, the time of arrival of the [^{15}O]butanol in the brain was determined by the steeply increasing deviation of the instantaneous count rates from zero in the list-mode data. Then, sixteen consecutive frames of 2 s each, obtained from the activation and control data, were used to calculate pair-wise subtractions (activation minus control). The subtraction frames included the time interval during which the measured cerebral activity in the activated areas was higher than in the non-activated areas of the brain (Wunderlich *et al.* 1998). Prior to subtraction, the images were spatially aligned using an automatic image realignment algorithm (Woods *et al.* 1993). No normalization of the image data was performed. From these subtraction frames, t-maps were calculated pixel by pixel. The pixels showing significant activation were determined in the t-maps after thresholding at a t-value of 2·947 ($P < 0{\cdot}01$, d.f. = 15). The centre of gravity of the pixels with the maximal t-value, indicating the location of the most consistent increase of cerebral blood flow, as determined in each subject (Wunderlich *et al.* 1998).

Anatomical localization of activity changes was done by co-registration of the PET images with the subject's magnetic resonance images using a spatial alignment algorithm (Steinmetz *et al.* 1992). Stereotactic co-ordinates were determined for the COG of the activations using the computerized brain atlas (Thurfjell *et al.* 1995).

RESULTS

Factors affecting accuracy and comparability of transcranial magnetic stimulation mapping

A representative example of TMS mapping of MEPs evoked in the right FDI is shown in Fig. 2. In general, mean amplitudes fell off gradually towards the borders of the stimulation area. However, when the target muscle was at rest, at least one local maximum was frequently identified in addition to the site of the maximal amplitude. This is illustrated in Fig. 2*A*, which demonstrates averaged EMG responses of the resting FDI muscle. Although a weak stimulation intensity of only 1·2 times resting motor threshold was used, MEPs could be evoked over several positions extended in the longitudinal as well as in the mediolateral axis. The map size enlarged on contraction of the target muscle at about 15% of maximal individual force (Fig. 2*B*), when the same stimulus intensity as in the resting condition was used. Figure 2*C* and *D* shows topographical changes of MEPs normalized to the maximal mean amplitude in the resting and activated condition.

Methodological aspects of two variables describing TMS-derived maps of muscle representations were investigated in more detail: COG, and the spatial extention, as defined by the number of T3Ps.

Dependence of the accuracy of the COG on the number of stimuli per stimulation site and the extension of the stimulation area

We calculated the accuracy of COG measurements as a function of the number of trials for mapping FDI in eleven subjects (Fig. 3*A* and *B*). The result obtained after twenty stimuli each at the maximal stimulation area covering at least forty-nine stimulus sites was regarded as the optimal estimate of the COG. Figure 3*A* shows, for three differently sized stimulation areas centred by pPOE, the distance of the calculated COG from the optimal estimate of COG with increasing number of trials. Figure 3*B* shows complementarily the accuracy of a COG estimate for three numbers of stimuli per site with increasing area of stimulation. With the maximal stimulation area, the mean difference COG was, after ten trials, on average within less than 1 mm (95% confidence interval of mean difference: 0·2–1·2 mm) of the best COG estimate and after five stimuli within 2 mm (95% confidence interval of mean difference: 0·6–2·4 mm) of the best COG estimate. If the number of stimuli was increased beyond ten per site, the estimate did not improve on average more than 0·2 mm (5 cm × 5 cm area) or 0·6 mm (7 cm × 7 cm area) or 0·8 mm (maximal area).

To investigate the possibility that performing successive stimulations at any site contributed to the relative stability of COG measurements, stimulations were pseudorandomized after each single trial in another three subjects. In these experiments a computer program selected the skull co-ordinates for the subsequent stimulation site from the set of stimulation sites where less than twenty stimuli had been delivered until twenty stimulations had been performed at any of the forty-nine sites. COG distance from optimal COG estimate decreased at a similar rate as in the standard stimulation protocol and fell below 1 mm after ten trials (not illustrated).

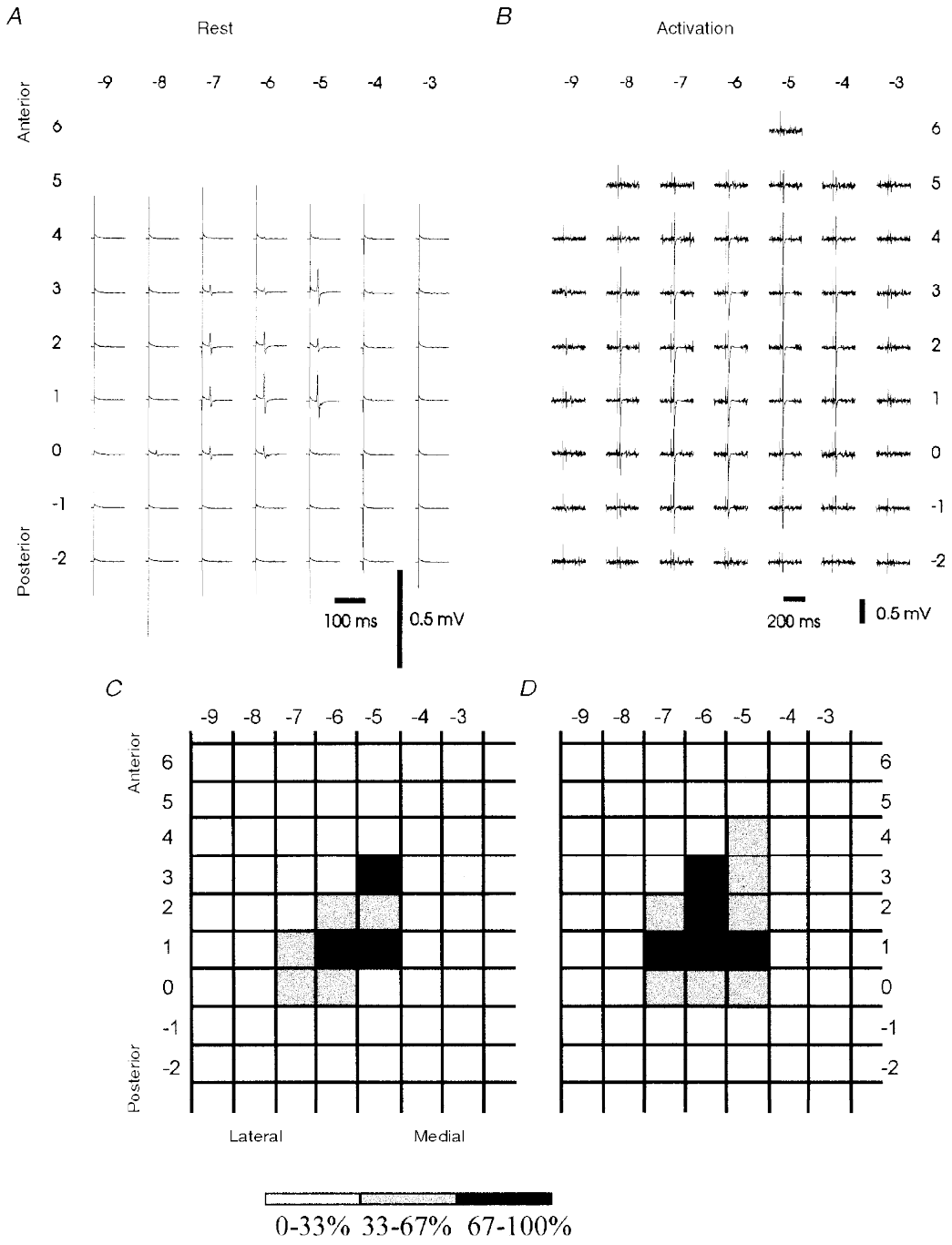

Figure 2. Example of MEP maps derived from stimulating 49 scalp positions overlying the left hemisphere in one subject

A and *B*, average of MEPs evoked in the relaxed (20 stimuli at each position) or slightly contracted (10 stimuli at each position) right FDI. Co-ordinates refer to positions (in cm) on the medio-lateral axis (from right to left) and on the fronto-occipital axis (from top to bottom). *C* and *D*, data normalized to the maximum mean amplitude of each map. Positions with a mean amplitude of at least 67 % of the maximum in black, positions with mean amplitudes between 33 and 67 % of the maximum amplitude in grey.

To estimate the spatial differences of COGs in two different measurements of the FDI at rest we calculated the COG positions from the averages of the first ten (1–10) trials and the second ten (11–20) trials in the three hemispheres examined with the coil repositioned between each trial, assuming that the first and the second set of ten trials were independent from each other. The mean difference of COGs ($COG_{1\text{-}10} - COG_{11\text{-}20}$) was $1{\cdot}9 \pm 0{\cdot}6$ mm. The difference of $COG_{1\text{-}10}$ and $COG_{11\text{-}20}$ was very similar when calculated on the twenty-two hemispheres mapped with twenty subsequent stimulations at each position ($1{\cdot}5 \pm 0{\cdot}8$ mm). This indicated that spatial differences greater than 3·1 mm ($1{\cdot}9 + 1{\cdot}2$ mm; mean + 2 S.D.) could be regarded as significant in an individual subject in any two maps within the same experimental session.

Influence of target muscle activation on COG

In addition to stimulation of the relaxed target muscle, we investigated the effect of a slight (about 15% of maximal force) pre-activation of the target muscle on the COG of the amplitude map. Such activation had previously been reported to lead to a systematic medial and anterior displacement of the COG in a study by Wilson and co-workers (Wilson *et al.* 1995). COG representations of three subjects are illustrated with the target muscle at rest and with slight pre-activation (Fig. 4). The mean 2-D distance of the COG with preactivation from the COG at rest was $2{\cdot}7 \pm 0{\cdot}2$ mm, but COG co-ordinates did not change systematically. Mean lateral deviation was $1{\cdot}0 \pm 1{\cdot}6$ mm.

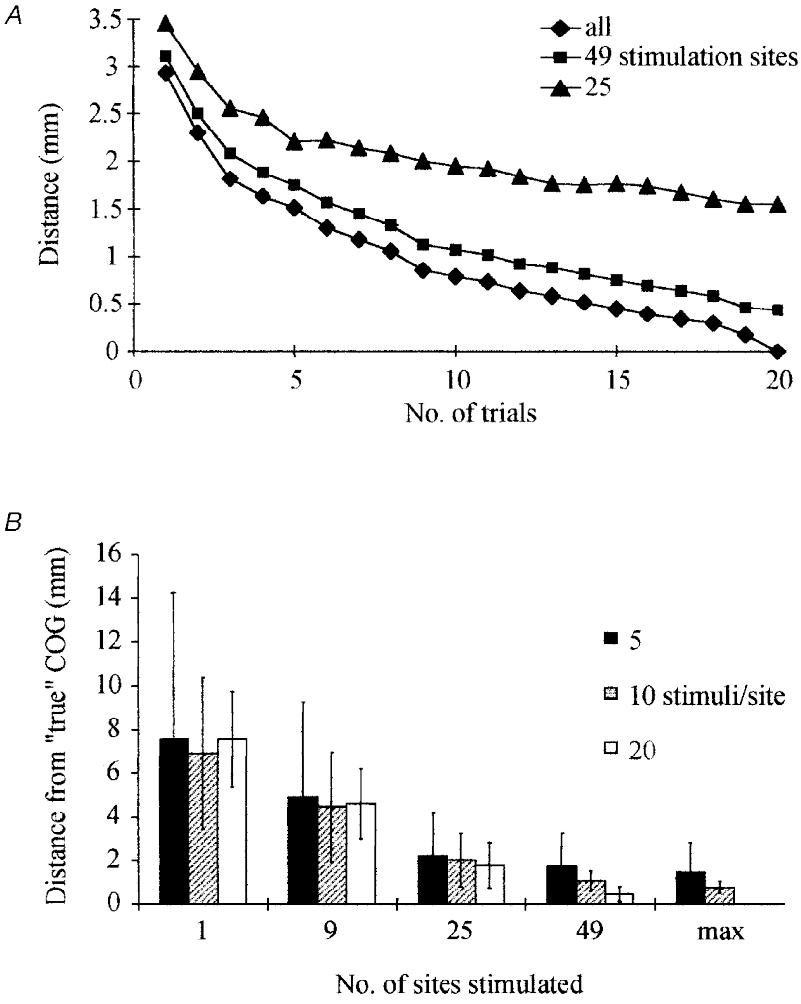

Figure 3. Dependence of accuracy of COG estimates on the number of stimulations applied at each position, and the extension of the stimulation area centred by the provisional point of optimal excitability

COGs are referenced to the COG computed using 20 stimulations per position and the most extended stimulation area. *A*, mean difference of COG calculated at an increasing number of trials for 3 extensions of stimulation area (5 cm × 5 cm, 7 cm × 7 cm, maximal area) from the optimal COG estimate. *B*, 95% confidence intervals for the mean difference from the optimal COG estimate for 3 numbers of trials (5, 10, 20) per position. Error bars represent S.E.M.

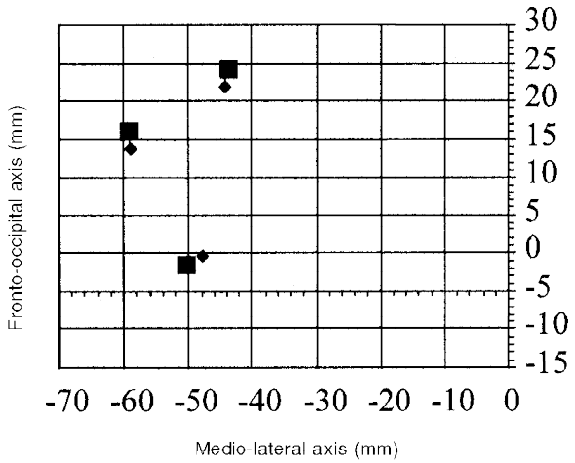

Figure 4. Effect of contraction of FDI on the COG
COG positions were determined for three subjects at rest (■) and at slight (15% of maximal force production) contraction (◆) of the target muscle.

Dependence of accuracy of number of top-third positions on number of stimuli per stimulation site

The spatial extension of maps was quantitatively assessed by the number of T3Ps. A position on the scalp was classified as a T3P when its stimulation produced a mean MEP amplitude greater than two-thirds of the maximal mean MEP amplitude. Despite the fact that the same relative stimulation intensity was used for each hemisphere and subject, the number of T3Ps varied considerably between different hemispheres and subjects (range 1 to 8). The mean number of T3Ps was $3{\cdot}5 \pm 2{\cdot}1$. Similar to estimating the accuracy of COG, we estimated the accuracy of the number of T3Ps after increasing numbers of trials, regarding the result obtained after twenty stimuli at each of at least forty-nine stimulus sites as the optimal estimate of the number of T3Ps. Ninety-five per cent confidence intervals for the mean

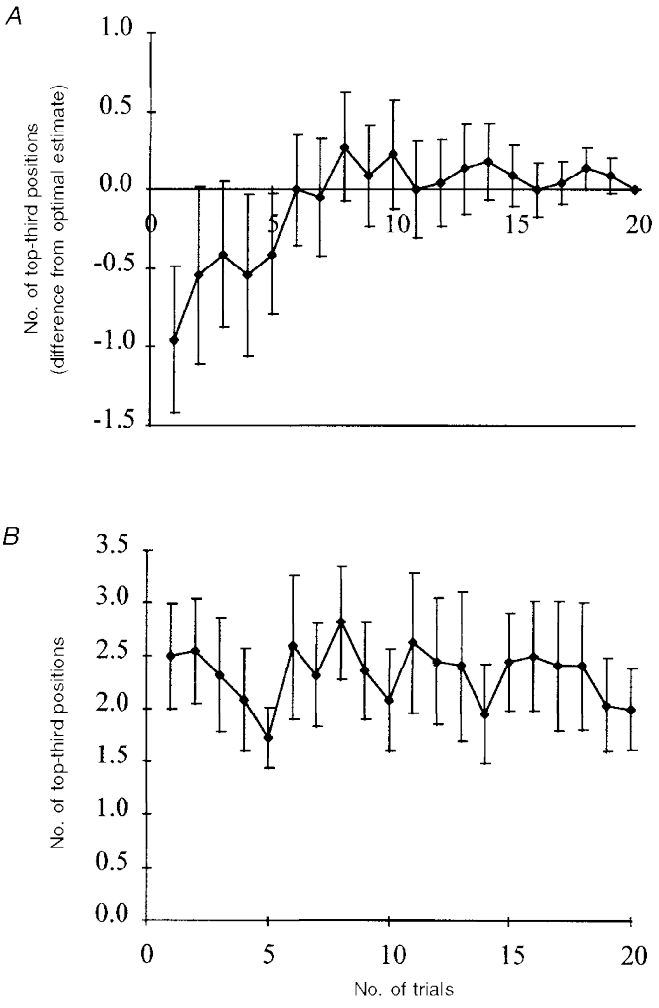

Figure 5. Dependence of accuracy of number of excitable scalp positions on the number of stimuli per stimulation site
Top-third positions (T3Ps) were defined as positions with a mean amplitude of at least 67% of the maximum mean amplitude. *A*, increase of the number of T3Ps with increasing number ($F = 1{\cdot}75$; $P < 0{\cdot}05$; ANOVA). Error bars indicate S.E.M. *B*, lack of order effect of number of T3Ps. Number of T3Ps remained essentially constant when analysed on successive sets of single trials.

Table 1. Co-ordinates of scalp positions of optimal excitability (POE) and COGs of MENT, FDI and AH in 11 subjects

		Left hemisphere		Right hemisphere	
	Muscle	Ant-post	Med-lat	Ant-post	Med-lat
POE					
	FDI	1·5 ± 1·2	5·0 ± 0·8	1·5 ± 1·0	−5·1 ± 1·1
	MENT	2·0 ± 0·8	8·5 ± 0·6	2·3 ± 0·5	−7·8 ± 1·0
	AH	0·8 ± 1·7	1·8 ± 0·5	−0·3 ± 1·0	−2·0 ± 0·8
COG					
	FDI	1·4 ± 0·8	5·0 ± 0·5	1·5 ± 0·7	−5·1 ± 1·1
	MENT	2·0 ± 0·7	8·7 ± 0·4	2·1 ± 0·6	−8·2 ± 0·6
	AH	0·4 ± 0·5	1·5 ± 0·5	0·1 ± 0·7	−1·4 ± 0·7

Ant-post, anteroposterior. Med-lat, mediolateral.

difference of the number of T3Ps from the number of T3Ps following twenty trials are shown as a function of the number of trials (Fig. 5*A*). There is an underestimation of the 'true' number of T3Ps with less than 8–10 trials. Since, by definition, the number of T3Ps cannot be underestimated in the case of an optimal estimate of only one T3P, the difference will probably be even greater than indicated by Fig. 5*A*. Using a one-way repeated measure analysis of variance (ANOVA), a statistically significant effect of trial number was found ($F = 1·75$; $P < 0·05$).

In order to investigate the possibility that stimulation at approximately 0·3 Hz altered the motor cortical excitability resulting in an increase in the number of T3Ps, we performed a trial-by-trial analysis of the number of T3Ps. We considered the twenty subsequent stimulations at a given position as independent from the twenty trials of the previous position, since the break between stimulation of different positions was sufficiently long to revert any short-term physiological effect with a time constant of a few seconds. We calculated the number of T3Ps for each of twenty sets of forty-nine trials separately. In this analysis, in contrast to the analysis of the cumulatively averaged MEP amplitudes, the number of T3Ps did not change significantly (repeated measures ANOVA) with trial number (Fig. 5*B*).

Scalp topography of motor-evoked potentials from FDI, MENT and AH

Laterality, handedness and somatotopy

The number of T3Ps was analysed for each hemisphere separately for FDI. The number of T3Ps on the dominant hemisphere correlated poorly with the number on the non-dominant hemisphere ($y = -0·0197x + 3·5225$; $r = 0·03$; n.s.). There was no difference in numbers of T3Ps when the left hemisphere (3·5 ± 2·5) was compared with the right (3·5 ± 1·6). There was also no statistically significant difference between the number of T3Ps over the dominant (3·7 ± 2·4) and the non-dominant (3·2 ± 1·7) hemisphere ($n = 11$; $P = 0·28$). Similar results were obtained when the cut-off threshold was set to one-third of the maximal mean MEP amplitude.

Figure 6 combines the mapping results of MEPs from FDI, MENT and AH in both hemispheres. Ellipses on both hemispheres indicate 95% confidence regions for COG skull positions of the three muscles. COG positions are highly symmetrical across the cerebral hemispheres. There was no

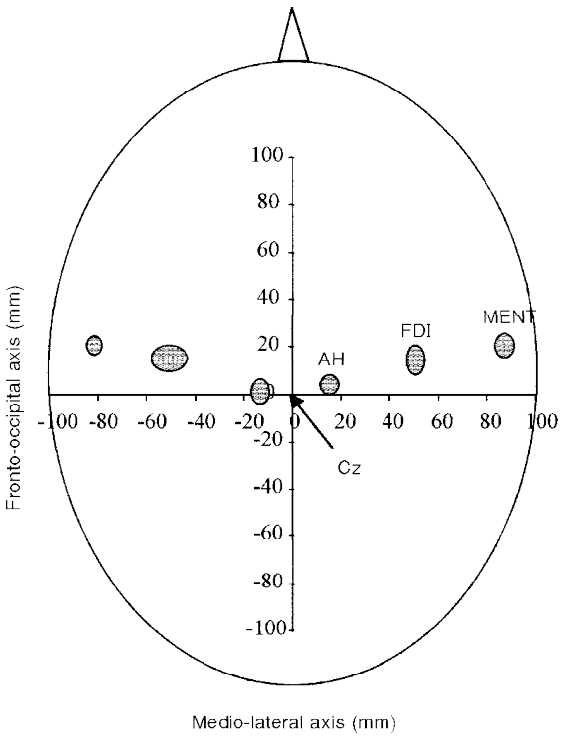

Figure 6. Topographical scalp distribution of 95% confidence regions of COGs

The shaded ellipses represent the distribution of MENT, FDI and AH regions in 11 subjects.

Table 2. Scalp co-ordinates of COGs computed following contralateral and ipsilateral stimulation of MENT in 3 subjects

	Left hemisphere		Right hemisphere	
Response	Ant-post	Med-lat	Ant-post	Med-lat
Contralateral	2·1 ± 0·6	−8·2 ± 0·6	2·0 ± 0·7	8·7 ± 0·4
Ipsilateral	2·1 ± 0·8	−8·2 ± 0·6	2·2 ± 0·4	8·8 ± 0·4

Ant-post, anteroposterior. Med-lat, mediolateral.

overlap of the 95% confidence regions of COG positions in the three muscles representing different body parts. AH, FDI and MENT regions follow a posterior–anterior gradient. Mean COG positions were similar to POE in all three muscles (Table 1).

Comparison of ipsilateral and contralateral representations of MENT

Results of mapping MENT are illustrated in three subjects (Fig. 7) in whom ipsilateral responses could be recorded. In the fourth subject, ipsilateral MEPs could not be evaluated because the magnetic coil generated a large artefact in the electrode overlying ipsilateral MENT. In general, the topographical distribution was more irregular and the variability of MEP amplitudes was greater for MENT than for FDI or AH. However, maps from contralateral and ipsilateral stimulation largely overlapped. COG co-ordinates following contralateral as well as ipsilateral stimulation were similar (Table 2), suggesting that the cortical elements producing responses in ipsilateral MENT were close to, or identical with, the elements producing contralateral responses. MEP amplitudes were smaller following ipsilateral compared with contralateral stimulation of the target muscle ($P < 0·001$, Student's paired t test). In addition to calculation of COGs, the number of T3Ps was evaluated as an arbitrary measure of the spatial extension of maps obtained by contralateral or ipsilateral transcranial stimulation. T3Ps were defined as above. Mean MEP amplitudes evoked by ipsilateral stimulation were normalized to the maximal mean amplitude following ipsilateral stimulation of the same muscle as well as to the maximal mean amplitude following contralateral stimulation. With contralateral stimulation there was no statistically significant difference between the number of T3Ps obtained by stimulation of the right and the left hemisphere (left hemisphere, 5·0 ± 1·4 positions; right hemisphere, 4·5 ± 0·7 positions; $n = 4$). When ipsilateral amplitudes were referenced to the maximal mean amplitude following contralateral stimulation of the same muscle, the number of T3Ps was significantly smaller when compared with contralateral stimulation (ipsilateral, 1·2 ± 1·2 positions; contralateral, 4·8 ± 1·0 positions; $P < 0·001$).

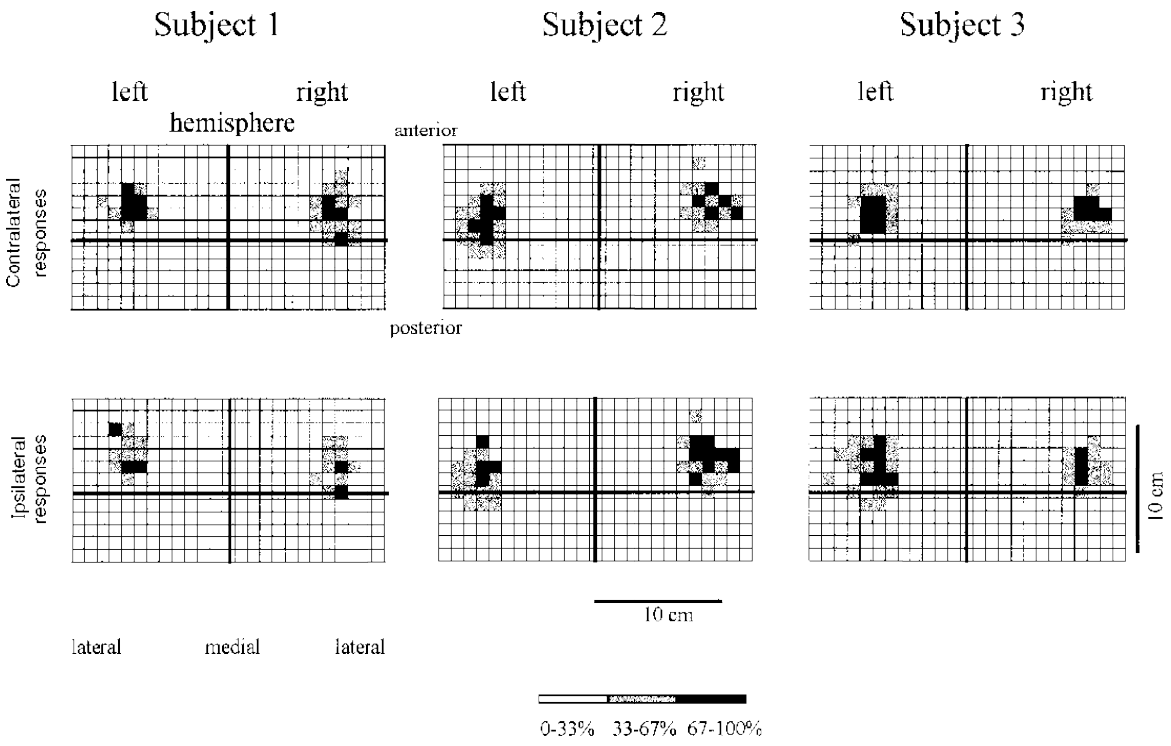

Figure 7. Response maps of MENT on contralateral (upper panels) and ipsilateral (lower panels) side

Results from 3 subjects. Continuous lines, representing the mid-sagittal (vertical line) and interaural (horizontal line) axes intersect at Cz. Amplitudes are given as a percentage of the maximal mean response amplitude following contralateral or ipsilateral stimulation, respectively.

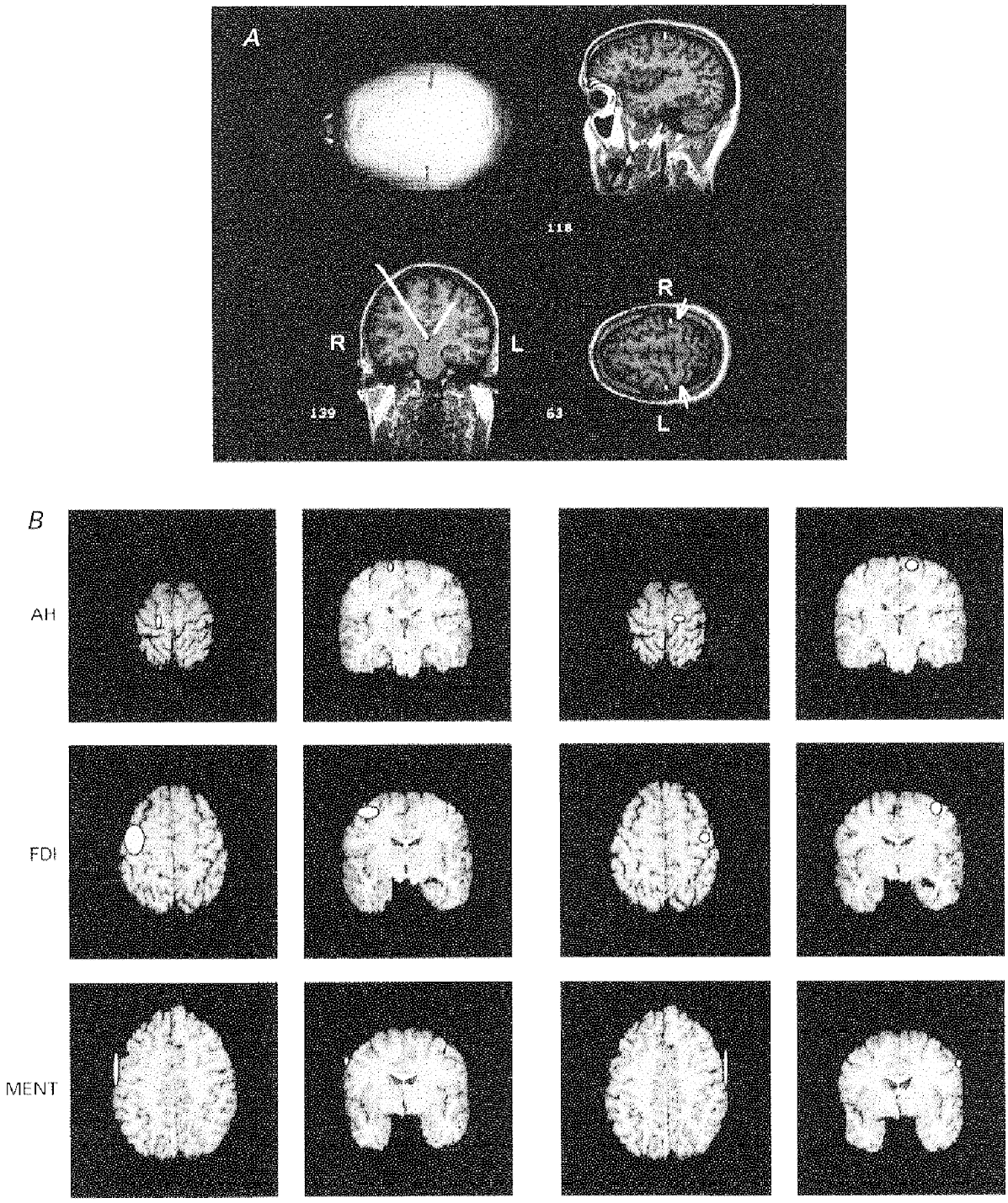

Figure 8. Integration of TMS and MR imaging

A, identification of co-ordinates of projections of COG onto the MR anatomy. The example is of FDI mapping in 1 subject. COG projections were viewed in 3 orthogonal planes of the MR images. The arrow indicates location of the central sulcus. The templates corresponding best to the MR planes were identified in the atlas of Talairach & Tournoux (1988) and the 3-D co-ordinates of the COG projection were determined where it entered the brain. R, right; L, left. *B*, regions of COG projections of right (first and second column of panels) and left (third and fourth column) AH, FDI and MENT (mean $\pm$ 2 S.D.) in sections of the standard brain (Roland & Zilles, 1994) oriented in parallel with the axial and coronal planes in the atlas of Talairach & Tournoux (1988).

Table 3. Stereotactic co-ordinates (Talairach & Tournoux, 1988) of COG projections derived from TMS mapping of FDI, MENT and AH

	Left hemisphere				Right hemisphere			
	n	*x*	*y*	*z*	*n*	*x*	*y*	*z*
FDI	14	-37 ± 6	-13 ± 8	53 ± 3	11	37 ± 3	-12 ± 5	53 ± 3
MENT	4	-56 ± 1	-7 ± 8	42 ± 1	4	55 ± 1	-5 ± 7	42 ± 1
AH	4	-15 ± 1	-23 ± 3	64 ± 2	4	12 ± 3	-22 ± 2	64 ± 3

This difference was exclusively due to the smaller amplitude of the maximal MEP size following ipsilateral stimulation, since the difference between the number of T3Ps became statistically insignificant when ipsilateral amplitudes were referenced to the maximal mean ipsilateral amplitude ($4{\cdot}7 \pm 2{\cdot}7$ positions; cf. Fig. 7).

Integration of TMS mapping data with structural and topographically located information from MRI and PET

Integration of TMS mapping data into brain anatomy

We adapted the method proposed by Wassermann *et al.* (1996) to identify the anatomical structures activated by TMS. After fitting an ellipsoid mathematically to each individual skull and transforming the individual 2-D co-ordinates of the MEP map into the 3-D MR brain (see Methods for details), COG projections were made by constructing a bar perpendicular to the surface of the ellipsoid. The Talairach co-ordinates of the COG projections were identified in three orthogonal brain slices. Talairach co-ordinates were identified directly at the site where the COG projection entered the brain (Fig. 8*A*). An analogous procedure was performed for all three muscles. Talairach co-ordinates of COG projections of FDI, MENT and AH are summarized for both hemispheres in Table 3. To visualize the locations of the COG projections on the brain surface, Talairach co-ordinates were superimposed onto the MR anatomy of a 'standard brain' (Roland & Zilles, 1994). The 'standard brain' has the advantage of preserving anatomical details in the presence of statistical accuracy and avoids substantial spatial blurring resulting from simply averaging structural brain images. The areas of the mean COG co-ordinates with 2 S.D. are shown for all three muscles in sections of the standard brain oriented in parallel to the axial and coronal sections of the atlas of Talairach & Tournoux (1988) (Fig. 8*B*). Volumes of COG of FDI and MENT lie within the precentral gyrus. Projections of AH lie anterior to the precentral gyrus, presumably because the zone of activation is buried within the interhemispheric fissure and is located along the extended projection of the COG.

Comparison of activation centres of TMS and PET

Finally, we examined how TMS-derived COG projections compared with the COG of the cerebral activation areas as evident from PET scanning. To combine PET and TMS results from several subjects quantitatively, mean Talairach co-ordinates (x, y, z; mean $\pm$ S.D.; mm) of the COG of the PET region maximally activated by repetitive index finger flexion were compared with mean co-ordinates derived from TMS mapping of FDI in the same subjects. PET COG co-ordinates (-33 ± 5, -19 ± 2, 54 ± 3) corresponded well with TMS COG co-ordinates (-37 ± 7, -16 ± 9, 53 ± 3). The 3-D spatial distance of the mean COGs was 4·7 mm. Individual data were plotted for lateral projections of TMS- and PET-derived COGs on the mid-sagittal plane of the Talairach atlas (Fig. 9*A*). Mean COG co-ordinates of PET and TMS mapping were projected onto the axial plane of the Talairach atlas nearest to the z-co-ordinate of both COGs (Fig. 9*B*). Mean COGs were both located in close proximity to each other on the posterior lip of the precentral gyrus.

DISCUSSION

Motor representation can be studied at different physiological, anatomical and behavioural spatial scales. If motor representation is observed in relation to large anatomical structures, the scale of observation may be termed a *macroscale of motor representation*. Clinically, this scale is used to localize the motor cortex presurgically. Often, in this approach the implicit methodological assumption is that all signals arise from a single site with little or no expansion (e.g. dipole analysis in EEG studies). In our study, this scale was used to compare TMS mapping results with the anatomy of the underlying cortex and with results obtained with cortical activation studies using PET.

If details of motor representation at a millimetre or submillimetre range are investigated, the scale of observation may be termed a *microscale of motor representation*. This scale can be approached by electrophysiological methods of mapping motor representations, which have recently been reviewed by Cheney (1996). The exact amount of the excited cortex depends on the methodological details of the stimulation technique used. As a rule, an increasingly sophisticated picture of the organization of the motor cortex emerges with smaller stimulation electrodes, and the intracortical microstimulation (ICMS) technique probably comes closest to an anatomical description of motor representation because it is least confounded by stimulus spread.

On the basis of the data presented above, we will argue that TMS maps can be reliably used to retrieve useful information on both scales of motor representation.

Macroscale representation: comparison of TMS maps to anatomy and PET activation studies

Using TMS, previous studies have investigated muscle representations of the upper extremity (Brasil-Neto *et al.* 1992*a*,*b*; Wilson *et al.* 1993) or muscles of the hand and the leg (Singh *et al.* 1997) and found a somatotopical arrangement of cortical muscle representation in agreement with the traditional homunculus extended over the lateral surface of the precentral gyrus (Penfield & Boldrey, 1937). Our results confirm and extend these findings using target muscles of three different body parts. We employed the centre-of-

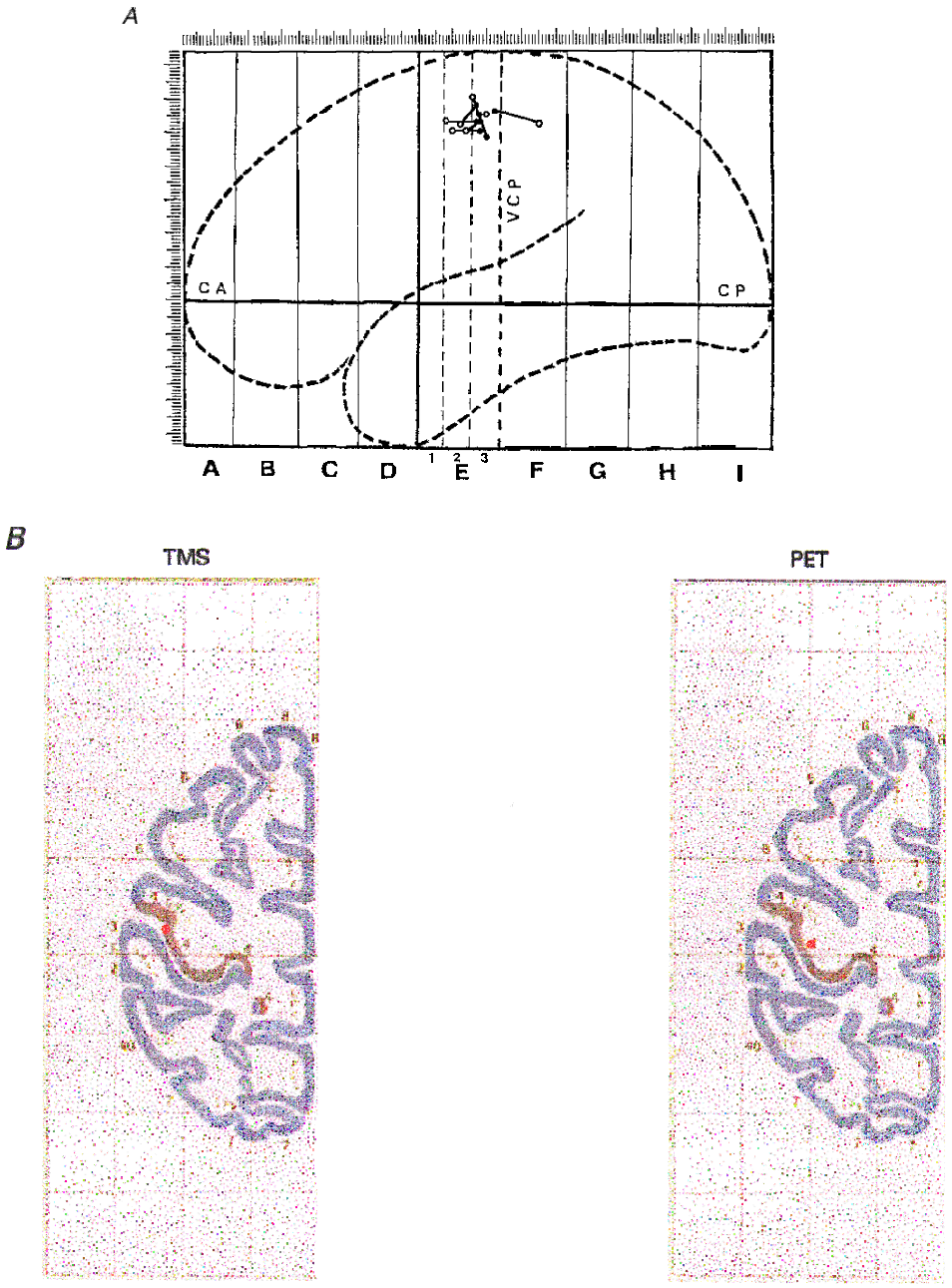

Figure 9. Integration of TMS and PET

A, Talairach co-ordinates (Talairach & Tournoux, 1988) of COG projections of TMS maps (right FDI; ○) and COG of the PET region metabolically activated by right index finger flexion (●) projected individually onto the mid-sagittal plane. Lines connect data from the same subject ($n = 7$). *B*, mean Talairach co-ordinates of COG projections of TMS maps (right FDI) and COG of regional activation (right index finger flexion; PET) projected onto the horizontal plane nearest to the z-co-ordinate in the atlas of Talairach & Tournoux (1988) ($n = 7$). Locations of COGs are indicated by the red dot. The dark area marks the posterior lip of the precentral gyrus.

gravity method (Wassermann *et al.* 1992, 1996) to integrate TMS maps with the underlying anatomy and metabolic activation studies. The mean COG projection of the FDI was located on the posterior lip of the precentral gyrus and close to the anatomical projection of the COG of the PET activation areas (Fig. 9). The location of the TMS projection corresponded to the location of the highest density of corticospinal neurones, and in particular, of the Betz cells, which are located in the posterior bank of the precentral gyrus (Porter & Lemon, 1995) and which are likely to be the anatomical origin of the fast-descending volleys generated by TMS. COG projections of TMS-derived maps and COGs of regional activation both lay on the posterior lip of the precentral gyrus and in close proximity to each other. TMS-derived COGs were located slightly anterior with respect to PET-derived COGs. One possibility would be that the site of excitation corresponded to the site of maximal magnetic field intensity, directly under the junction of the coil, rather than to the site of the virtual cathode as determined in preliminary experiments on peripheral nerves and used in the present study. Because the location of the virtual cathode was only 1 mm away from the junction of the coil, this difference would not provide a sufficient explanation. One could also argue that the different location of TMS-derived COGs could be due to the fact that the TMS maps were obtained in the relaxed state, and the PET maps in the activated state. This possibility is unlikely because muscle activation did not induce a systematic anterior displacement of TMS-derived COGs (Fig. 4). Instead, we suggest that the more posterior location of the PET-derived COGs results from the fact that TMS maps indicate activation of the motor output system, while the area of metabolic activation in PET reflects activity of both the motor output circuits as well as of the reafferent activity in the primary somatosensory cortex.

TMS mapping has been compared with structural anatomy and functional brain activation as assessed by imaging techniques in three recent studies (Wassermann *et al.* 1996; Krings *et al.* 1997; Singh *et al.* 1997). Of these, only the study by Wassermann *et al.*, using the method of projecting the TMS-derived COGs into the brain, showed a clear anatomical correspondence of the site of TMS activation with the precentral gyrus. Because Krings *et al.* (1997) used the POE, rather than the COG, to integrate TMS maps with anatomy, the projection was found to overlay the postcentral gyrus (cf. their Fig. 1). Since the boundaries of TMS-derived maps and those generated by functional activation studies are both defined by arbitrary thresholds, it seems more appropriate to compare the spatial co-ordinates of their COGs rather than the location of the TMS-derived COG in a spatially extended functional activation map. Such a comparison is lacking in previously published studies. Thus the present findings, although in general confirming previous findings of correlational analyses (Wassermann *et al.* 1996; Krings *et al.* 1997; Singh *et al.* 1997), extend those findings in demonstrating a high degree of correspondence between TMS-derived and PET-derived COGs.

TMS mapping has been advocated as a tool to identify the motor cortex presurgically. Integration of TMS maps with anatomy involves many intermediate steps each of which adds to spatial inaccuracies. Therefore we believe that for surgical purposes, the accuracy of individual anatomo-physiological integration should be improved by precise acquisition of positional coil data. This approach was used by Wassermann *et al.* (1996). In our view, there is no real advantage in visualizing on line the position of the stimulating coil in an MR data set obtained prior to the investigation (Krings *et al.* 1997) if the accuracy of the transformation procedure rests on only three landmarks. Even with highly accurate integration methods mapping results in surgical patients should be interpreted with caution, since there are only anecdotal reports of the validity of the TMS mapping technique under the circumstances of a grossly distorted anatomy (Krings *et al.* 1997). This issue also becomes important when TMS is used outside the motor cortex, and in particular as an interventional, rather than as a probing tool.

Microscale representation: methodological constraints and spatial aspects of TMS maps

In humans, the TMS mapping technique has been employed to investigate motor cortical plasticity (Pascual-Leone *et al.* 1995; Cohen *et al.* 1996; Rijntjes *et al.* 1997). In some studies employing TMS mapping, implicit assumptions have been made concerning the spatial interpretation of maps generated by TMS. However, some principles of how TMS maps are influenced have apparently been neglected. The principal cortical factor determining size and shape of TMS-derived maps is excitability of the stimulated region. For example, at a fixed stimulus intensity, the number of scalp positions from which MEPs can be evoked increases with increasing excitability of the cortical elements generating corticospinal commands. Similarly, the number of positions will increase with larger stimulus intensity. A simple demonstration that the spatial information is not readily available from TMS maps is evident from studies projecting MEP amplitude maps directly onto MRI scans (Levy *et al.* 1991; Krings *et al.* 1997). Clearly, corticospinal commands targeting α-motoneurons cannot arise from all the cortical sites from which the corresponding overlying scalp positions yielded EMG responses. Another example of an overly simple interpretation of TMS-generated maps is claims that different muscles have overlapping representational cortical areas (Verhagen Metman *et al.* 1993), since physical stimulus spread would cause a similar overlap of maps if the commands to the muscles originated from small and non-overlapping anatomical regions. TMS clearly cannot resolve the mosaic-like micro-organisation of the motor cortex in as much detail as revealed by single-neurone recordings or ICMS, because of the physical dimensions of the magnetic and the electric field induced within the cortex. Given the dimensions of physical and biological stimulus spread, it is a reasonable question whether TMS maps can at all justifiably be used to retrieve any detailed spatial information on the

microscale level of the motor cortex. Indeed, Ridding & Rothwell (1997) have argued that, in paradigms of motor plasticity, TMS maps cannot distinguish between effects on the organization of the cortex and on changes in excitability.

The spatial extension of the anatomical hand representation in the primary motor cortex is not known in humans. Nudo & Masterton (1990) measured the size of the anatomical sources of the corticospinal tract in mammals from twenty-two different species. They found that the amount of corticospinal tract cortex is closely related to the total amount of neocortex and that the relationship of the amount of corticospinal tract cortex to total cortex is constant along the anthropoid lineage. The same constancy was observed for the ratio of the subregion containing Brodmann area 4 to total amount of neocortex (see their Fig. 5), but the ratio for anatomical size of area 4 to total amount of neocortex was not investigated. If the same rule were applicable to area 4 itself, then an estimate of the size of human anatomical forearm representation could be made using an ICMS approximation of anatomical representation in squirrel monkeys (Nudo *et al.* 1992, 1996): the average spatial extent of the squirrel monkey forearm representation was 9·69 mm^2 (Nudo *et al.* 1992) to 12·08 mm^2 (Nudo *et al.* 1996). The squirrel monkey neocortex has an approximate area of 2150 mm^2 (Nudo & Masterton, 1990). The human neocortex (220 000 mm^2; Zenker, 1985) is approximately 100 times larger than the squirrel monkey cortex and therefore the human motor cortical forearm representation would have an extension of around 970–1210 mm^2 (or from 3·1 cm × 3·1 cm to 3·5 cm × 3·5 cm). This estimate neglects minor inaccuracies resulting from using ICMS as an approximation of anatomical representation. Although human area 4 is partially buried in the anterior wall of the central sulcus, where it may be less excitable by low-intensity TMS, a part of it is exposed at the crest of the precentral gyrus and oriented in parallel with the skull surface (Zilles *et al.* 1995). TMS presumably activates corticospinal neurones transsynaptically via horizontal afferent projections (Rothwell, 1997) and the distance that those projections can travel within the cortex is a few millimetres (Huntley, 1997).

The minimum spatial resolution of TMS (i.e. the smallest distance at which a difference in amplitude of the evoked potentials can be reliably recognized) has been estimated to be 5 mm in previous mapping studies (Brasil-Neto *et al.* 1992*b*). This methodological spatial resolution does not directly reflect a spatial resolution of the excited cortical area. However, it is important to note that its dimension and the magnitude of the variability of COG measurements found in the present study are substantially below the above estimates of anatomical size of the origin of the corticospinal tract targeting α-motoneurons of the small hand and finger muscles. Thus, TMS maps are indeed likely to contain information on the spatial organization of the underlying cortex if certain methodological constraints are observed (see below). These conclusions are also in agreement with experimental findings that the number of excitable scalp positions can increase in the absence of changes in spinal excitability and alterations of motor threshold at the POE (Cohen *et al.* 1996).

How can this 'microscale' spatial information be retrieved? For reasons outlined above, there is no direct way to calculate the dimensions of the excited area from the dimensions of the TMS maps. Changes in excitability and spatial changes, associated with experimental conditions, can be partially disentangled by using fixed multiples of motor threshold during mapping or by using normalized maps. In this approach, arbitrary thresholds are used to define spatial borders. The number of positions meeting a certain relative threshold criterion will remain constant if excitability changes homogeneously within an excitable area and if the extension of that area remains constant. Conversely, the number of positions will increase if (i) excitability at the point of maximum excitability remains constant and the active area enlarges, or (ii) the increase in excitability at the point of maximum excitability is less than at the neighbouring sites. In the present study, we did not systematically explore the dependence of the number of excitable positions on the arbitrary threshold. However, the T3P measure seems to maintain a balance between two requirements of an arbitrary threshold: sensitivity to spatial changes in excitability and reasonable relationship to the size of the excitable nervous tissue.

While the *number of positions* associated with amplitudes exceeding an arbitrary threshold is likely to be sensitive to a symmetrical spatial expansion of excitability within or outside the original representational area, the *centre of gravity* (e.g. Wilson *et al.* 1993, 1996), on the other hand, is likely to be a measure of relative shifts in excitability within the representational area, as well as of an asymmetric expansion. Surprisingly, neither of the two variables has previously been sufficiently characterized.

The dependence of COG accuracy and number of T3Ps on stimulation parameters lead to specific methodological constraints when experimental differences of maps are investigated. For TMS mapping of different successive experimental conditions (e.g. prior to and following an intervention), it is safe to apply parameters for which the confidence region of the mean COG distance from the optimal COG estimate is smaller than the expected change in COG. For example, to detect a mean COG difference of 1 mm, preferably ten trials per site and a maximally extended stimulation area should be used. However, in an individual subject, as was argued above, using ten trials per site and a maximal extension of the stimulation area, only a distance in COGs greater than 3·1 mm in any two successive sessions would indicate a significant change of COG positions. Similarly, at least eight to ten stimuli per site must be used to estimate the number of T3Ps correctly in a group of subjects. Extending the stimulated field to positions where no responses could be elicited occasionally yielded a substantial improvement in accuracy of COG when compared with calculations of COG based on a fixed 7 cm × 7 cm area of

stimulation. Therefore it seems appropriate, for future mapping studies, to recommend the use of maximally extended stimulation areas rather than a fixed radius around the pPOE. There was no advantage of completely randomizing the site of magnetic stimuli as opposed to finishing the set of trials first on one site before moving on to the next site. Using the above-listed parameters, a TMS map can be completed relatively quickly and it is feasible to investigate multiple experimental conditions in an individual subject. Does the TMS mapping procedure influence its own results? It has been shown that repetitive cortical stimulation at frequencies of about 1 Hz leads to a change of cortical representational maps and excitability (Nudo *et al.* 1990). In our study, using stimulation frequencies around 0·3 Hz, the number of T3Ps was independent of the trial order, supplying indirect evidence that TMS mapping induced no cortical excitability changes at this stimulation frequency.

Handedness and somatotopy

ICMS studies in monkeys have shown a larger representation of hand muscles on the dominant as compared with the non-dominant hemisphere (Nudo *et al.* 1992). In humans, the size of the precentral gyrus differs between the dominant and the non-dominant hemisphere (Amunts *et al.* 1996). Lower motor thresholds, indicating an increased cortical excitability of dominant hand muscles, have previously been found by employing TMS in humans (Triggs *et al.* 1994). Furthermore, the dominant hand occupied a larger area of the cortex in a recent study combining fMRI and TMS (Krings *et al.* 1997). In another TMS study, however, no significant differences were found in a number of variables comparing dominant with non-dominant hand muscle representation (Cicinelli *et al.* 1997). In our study, there was a trend toward a greater number of T3Ps on the dominant hemisphere, but the difference was not significant. It is likely that the lack of clear differences between the dominant and the non-dominant hemisphere found in our study and in the study by Cicinelli and co-workers (1997) results from the fact that a substantial, and presumably interindividually variable part of Brodmann area 4 controlling hand movements is buried in the intrasulcal surface of the precentral gyrus where the cortical output elements are less readily excited by TMS (Rothwell, 1997). Indeed, it is the intrasulcal surface where the differences between dominant and non-dominant hemispheres have been found morphometrically (Amunts *et al.* 1996).

It has previously been shown that both ipsilateral and contralateral cortical stimulation evoke responses in facial muscles suggesting that the corticonuclear tract projects bilaterally to the corresponding motoneurons. In single motor unit studies, evidence was found for an oligosynaptic corticobulbar pathway projecting mainly contralaterally as well as for a polysynaptic pathway projecting bilaterally (Meyer *et al.* 1994). However, it remains unclear whether ipsilateral and contralateral projections have spatially separate cortical representations. Therefore it is remarkable that the mean COGs of ipsilateral and contralateral facial muscle representations were virtually identical. This may indicate that ipsi- and contralateral facial muscle representations share the same neuronal substrates. In this respect, facial muscles differ from small hand muscles, since two spatially distinct zones have been found for ipsilateral and contralateral FDI representations (Wassermann *et al.* 1994).

Centres of gravity at target muscle relaxation *versus* preactivation

Using slightly different stimulation parameters, we have confirmed previous studies demonstrating a difference of COGs of the relaxed as compared with the contracted muscle (Wilson *et al.* 1995). In our study, the mean 2-D distance of the COG with preactivation from the COG at rest was $2{\cdot}7 \pm 0{\cdot}2$ mm and, thus fell outside the 95% confidence interval for the mean difference of COG measurement from the optimal COG estimate at the stimulation parameters used. COG co-ordinates, however, did not change systematically in the lateromedial direction. The mean deviation along the coronal axis was only $1{\cdot}0 \pm 1{\cdot}6$ mm and substantially less than the approximately 6 mm medial displacement of the COG induced by contraction of the APB observed by Wilson and co-workers (1995). A possible reconciliation of the two apparently diverging results could be that the COG of thumb muscle representation is located at the lateral border of the finger representation while the muscles subserving the index finger are located preferentially towards the centre of the finger representation (Penfield & Boldrey, 1937). If recruitment of additional neuronal elements with preactivation were confined to the upper limb representation (see e.g. Donoghue & Sanes, 1994), the thumb (APB) representation would have to expand medially while the index finger (FDI) representation could expand in both directions.

Amunts, K., Schlaug, G., Schleicher, A., Steinmetz, H., Dabringhaus, A., Roland, P. E. & Zilles, K. (1996). Asymmetry in the human motor cortex and handedness. *Neuroimage* **4**, 216–222.

Brasil-Neto, J. P., Cohen, L. G., Panizza, M., Nilsson, J., Roth, B. J. & Hallett, M. (1992*a*). Optimal focal transcranial magnetic activation of the human motor cortex: effects of coil orientation, shape of the induced current pulse, and stimulus intensity. *Journal of Clinical Neurophysiology* **9**, 132–136.

Brasil-Neto, J. P., McShane, L., Fuhr, P., Hallett, M. & Cohen, L. G. (1992*b*). Topographic mapping of the human motor cortex with magnetic stimulation: factors affecting accuracy and reproducibility. *Electroencephalography and Clinical Neurophysiology* **85**, 9–16.

Cheney, P. D. (1996). Electrophysiological methods for mapping brain motor and sensory circuits. In *Brain Mapping: The Methods*, ed. Toga, A. W. & Maziotta, J., pp. 277–309. Academic Press, San Diego.

Cicinelli, P., Traversa, R., Bassi, A., Scivoletto, G. & Rossini, P. M. (1997). Interhemispheric differences of hand muscle representation in human motor cortex. *Muscle and Nerve* **20**, 535–542.

Classen, J., Knorr, U., Werhahn, K. J., Schlaug, G., Schnitzler, A., Steinmetz, H., Seitz, R. J. & Benecke, R. (1995). Integration of neurophysiological, anatomical and metabolic brain information on cortical motor representation. *Human Brain Mapping*, suppl. 1, 282.

Cohen, L. G., Gerloff, C., Faiz, L, Uenishi, N., Classen, J., Liepert, J. & Hallett, M. (1996). Directional modulation of motor cortex plasticity induced by synchronicity of motor outputs in humans. *Society for Neuroscience Abstracts* **22**, 1452.

Donoghue, J. P. & Sanes, J. N. (1994). Motor areas of the cerebral cortex. *Journal of Clinical Neurophysiology* **11**, 382–396.

Herzog, H., Seitz, R. J., Tellmann, L., Rota Kops, E., Julicher, F., Schlaug, G., Kleinschmidt, A. & Müller-Gartner, H. W. (1996). Quantitation of regional cerebral blood flow with ^{15}O-butanol and positron emission tomography in humans. *Journal of Cerebral Blood Flow and Metabolism* **16**, 645–649.

Huntley, G. W. (1997). Correlation between patterns of horizontal connectivity and the extent of short-term representational plasticity in rat motor cortex. *Cerebral Cortex* **7**, 143–156.

Karni, A., Meyer, G., Jezzard, P., Adams, M. M., Turner, R. & Ungerleider, L. G. (1995). Functional MRI evidence for adult motor cortex plasticity during motor skill learning. *Nature* **377**, 155–158.

Krings, T., Buchbinder, B. R., Butler, W. E., Chiappa, K. H., Jiang, H. J., Cosgrove, G. R. & Rosen, B. R. (1997). Functional magnetic resonance imaging and transcranial magnetic stimulation: complementary approaches in the evaluation of cortical motor function. *Neurology* **48**, 1406–1416.

Levy, W. J., Amassian, V. E., Schmid, U. D. & Jungreis, C. (1991). Mapping of motor cortex gyral sites non-invasively by transcranial magnetic stimulation in normal subjects and patients. In *Magnetic Motor Stimulation*: *Basic Principles and Clinical Experience*, ed. Levy, W. J., Cracco, R. Q., Barker, A. T. & Rothwell, J. *Electroencephalography and Clinical Neurophysiology*, suppl. 43. Elsevier Science Publishers, B.V., Amsterdam.

Meyer, B. U., Werhahn, K., Rothwell, J. C., Roericht, S. & Fauth, C. (1994). Functional organisation of corticonuclear pathways to motoneurons of lower facial muscles in man. *Experimental Brain Research* **101**, 465–472.

Nudo, R. J., Jenkins, W. M. & Merzenich, M. M. (1990). Repetitive microstimulation alters the cortical representation of movements in adult rats. *Somatosensory and Motor Research* **7**, 463–483.

Nudo, R. J., Jenkins, W. M., Merzenich, M. M., Prejean, T. & Grenda, R. (1992). Neurophysiological correlates of hand preference in primary motor cortex of adult squirrel monkeys. *Journal of Neuroscience* **12**, 2918–2947.

Nudo, R. J. & Masterton, R. B. (1990). Descending pathways to the spinal cord, IV: Some factors related to the amount of cortex devoted to the corticospinal tract. *Journal of Comparative Neurology* **296**, 584–597.

Nudo, R. J., Milliken, G. W., Jenkins, W. M. & Merzenich, M. M. (1996). Use-dependent alterations of movement representations in primary motor cortex of adult squirrel monkeys. *Journal of Neuroscience* **16**, 785–807.

Ojemann, J. G. & Silbergeld, D. L. (1995). Cortical stimulation mapping of phantom limb rolandic cortex. *Journal of Neurosurgery* **82**, 641–644.

Oldfield, R. C. (1971). The assessment and analysis of handedness: the Edinburgh inventory. *Neuropsychologia* **9**, 97–113.

Pascual-Leone, A., Dang, N., Cohen, L. G., Brasil-Neto, J. P., Cammarota, A. & Hallett, M. (1995). Modulation of muscle responses evoked by transcranial magnetic stimulation during the acquisition of new fine motor skills. *Journal of Neurophysiology* **74**, 1037–1045.

Penfield, W. & Boldrey, E. (1937). Somatic motor and sensory representation in the cerebral cortex of man as studied by electrical stimulation. *Brain* **60**, 389–443.

Porter, R. & Lemon, R. (1995). *Corticospinal Function and Voluntary Movement.* Clarendon Press, Oxford.

Rao, S. M., Binder, J. R., Hammeke, T. A., Banettini, P. A., Bobholz, J. A., Frost, J. A., Myklebust, B. M., Jacobson, R. D. & Hyde, J. S. (1995). Somatotopic mapping of the human primary motor cortex with functional magnetic resonance imaging. *Neurology* **45**, 919–924.

Ridding, M. C. & Rothwell, J. C. (1997). Stimulus/response curves as a method of measuring motor cortical excitability in man. *Electroencephalography and Clinical Neurophysiology* **105**, 340–344.

Rijntjes, M., Tegenthoff, M., Liepert, J., Leonhardt, G., Kotterba, S., Müller, S., Kiebel, S., Malin, J.-P., Diener, H.-C. & Weiller, C. (1997). Cortical reorganization in patients with facial palsy. *Annals of Neurology* **41**, 621–630.

Roland, P. E. & Zilles, K. (1994). Brain atlases – a new research tool. *Trends in Neurosciences* **17**, 458–467.

Rota Kops, E., Herzog, H., Schmid, A., Holte, S. & Feinendegen, L. E. (1990). Performance characteristics of an eight-ring whole body PET scanner. *Journal of Computer Assisted Tomography* **14**, 437–445.

Rothwell, J. C. (1997). Techniques and mechanisms of action of transcranial stimulation of the human motor cortex. *Journal of Neuroscience Methods* **74**, 113–122.

Schlaug, G., Knorr, U. & Seitz, R. J. (1994). Inter-subject variability of cerebral activations in acquiring a motor skill: a study with positron emission tomography. *Experimental Brain Research* **98**, 523–534.

Seitz, R. J., Huang, Y., Knorr, U., Tellmann, L., Herzog, H. & Freund, H.-J. (1995). Large-scale plasticity of the human motor cortex. *NeuroReport* **6**, 742–744.

Singh, K. D., Hamdy, S., Aziz, Q. & Thompson, D. G. (1997). Topographic mapping of trans-cranial magnetic stimulation data on surface rendered MR images of the brain. *Electroencephalography and Clinical Neurophysiology*, **105**, 345–351.

Steinmetz, H., Fürst, G. & Meyer, B. U. (1989). Craniocerebral topography within the international 10–20 system. *Electroencephalography and Clinical Neurophysiology* **72**, 499–506.

Steinmetz, H., Huang, Y., Seitz, R. J., Knorr, U., Schlaug, G., Herzog, H., Hacklander, T. & Freund, H.-J. (1992). Individual integration of positron emission tomography and high-resolution magnetic resonance imaging. *Journal of Cerebral Blood Flow and Metabolism* **12**, 919–926.

Talairach, J. & Tournoux, P. (1988). *Co-planar Stereotaxic Atlas of the Human Brain.* Thieme, Stuttgart.

Thurfjell, L., Bohm, C. & Bengtsson, E. (1995). CBA – an atlas-based software tool used to facilitate the interpretation of neuroimaging data. *Computer Methods and Programs in Biomedicine* **47**, 51–71.

Triggs, W. J., Calvanio, R., Macdonell, R. A., Cros, D. & Chiappa, K. H. (1994). Physiological motor asymmetry in human handedness: evidence from transcranial magnetic stimulation. *Brain Research* **636**, 270–276.

Verhagen Metman, L., Bellevich, J. S., Jones, S. M., Barber, M. D. & Streletz, L. J. (1993). Topographic mapping of human motor cortex with transcranial magnetic stimulation: homunculus revisited. *Brain Topography* **6**, 13–19.

Walter, H., Kristeva, R., Knorr, U., Schlaug, G., Huang, Y., Steinmetz, H., Nebeling, B., Herzog, H. & Seitz, R. J. (1992). Individual somatotopy of primary sensorimotor cortex revealed by intermodal matching of MEG, PET, and MRI. *Brain Topography* **5**, 183–187.

Wang, B., Toro, C., Wassermann, E. M., Zeffiro, T. A., Thatcher, R. W. & Hallett, M. (1994). Multimodal integration of electrophysiological data and brain images: EEG, MEG, TMS, MRI and PET. In *Functional Neuroimaging – Technical Foundations*, ed. Thatcher, R. W., Hallett, M., Zeffiro, T., Roy, J. E. & Huerta, M., pp. 251–257. Academic Press, London.

Wassermann, E. M., Pascual-Leone, A. & Hallett, M. (1994). Cortical motor representation of the ipsilateral hand and arm. *Experimental Brain Research* **100**, 121–132.

Wassermann, E. M., Wang, B., Toro, C., Zeffiro, T. A., Valls-Sole, J., Pascual-Leone, A. & Hallett, M. (1992). Projecting transcranial magnetic stimulation maps into brain MRI. *Society for Neuroscience Abstracts* **18**, 939.

Wassermann, E. M., Wang, B., Zeffiro, T. A., Sadato, N., Pascual-Leone, A., Toro, C. & Hallett, M. (1996). Locating the motor cortex on the MRI with transcranial magnetic stimulation and PET. *Neuroimage* **3**, 1–9.

Wilson, S. A., Thickbroom, G. W. & Mastaglia, F. L. (1993). Transcranial magnetic stimulation mapping of the motor cortex in normal subjects. The representation of two intrinsic hand muscles. *Journal of the Neurological Sciences* **118**, 134–144.

Wilson, S. A., Thickbroom, G. W. & Mastaglia, F. L. (1995). Comparison of the magnetically mapped corticomotor representation of a muscle at rest and during low-level voluntary contraction. *Electroencephalography and Clinical Neurophysiology*, **97**, 246–250.

Woods, R. P., Mazziotta, J. C. & Cherry, S. R. (1993). MRI-PET registration with automated algorithm. *Journal of Computer Assisted Tomography* **17**, 536–546.

Wunderlich, G., Knorr, U., Stephan, K. M., Tellmann, L., Azari, N. P., Herzog, H. & Seitz, R. J. (1998). Dynamic scanning of ^{15}O-butanol with positron emission tomography can identify regional cerebral activations. *Human Brain Mapping* **5**, 364–378.

Yousry, T. A., Schmid, D. U., Jassoy, A. G., Schmidt, D., Eisner, W. E., Reulen, H.-J., Reiser, M. F. & Lissner, J. (1995). Topography of the cortical motor hand area: prospective study with functional MR imaging and direct motor mapping at surgery. *Radiology*, **195**, 23–29.

Zenker, W. (ed.) (1985). Makroskopische Anatomie des Endhirns. In *Makroskopische und mikroskopische Anatomie des Menschen*, vol. 3, *Nervensystem, Haut und Sinnesorgane*, chap. 10, pp. 149–169. Urban & Schwarzenberg, Munich.

Zilles, K., Schlaug, G., Matelli, M., Luppino, G., Schleicher, A., Qu, M., Dabringhaus, A., Seitz, R. & Roland, P. E. (1995). Mapping of human and macaque sensorimotor areas by integrating architectonic, transmitter receptor, MRI and PET data. *Journal of Anatomy* **187**, 515–537.

Acknowledgements

We would like to thank R. J. Nudo PhD, for helpful discussions. This work was supported by Deutsche Forschungsgemeinschaft SFB 194 and grant Cl 95/2-2.

Corresponding author

J. Classen: Zentrum für Nervenheilkunde, Neurologische Klinik und Poliklinik, Universität Rostock, Gehlsheimer Strasse 20, 18055 Rostock, Germany.

Email: joseph.classen@med.uni-rostock.de